Hamburger Beiträge
zur Angewandten Mathematik

Dynamical Phenomena induced by Bottlenecks

Ingenuin Gasser and Bodo Werner

Nr. 2009-14
November 2009

DYNAMICAL PHENOMENA INDUCED BY BOTTLENECK

I. GASSER AND B. WERNER

Abstract. We study a microscopic follow-the-leader model on a circle of length L with a bottleneck. Allowing large bottleneck strengths we encounter very interesting traffic dynamics. Different types of waves - traveling and standing waves and combinations of both wave types - are observed. The way to find these phenomena requires a good understanding of the complex dynamics of the underlying (nonlinear) equations. Some of the phenomena, like the Ponies-on-a-Merry-Go-Round-solutions (POMs) are mathematically well known from completely different applications. Mathematically speaking we use Poincaré maps, bifurcation analysis and continuation methods beside numerical simulations.

Key words. traffic flow, numerical bifurcation analysis, Hopf bifurcation, Neimark–Sacker bifurcation, periodical solutions , standing waves, traveling waves

AMS subject classifications. 37M20, 65L07, 65P30, 65P40

1. Introduction. In recent decades many authors have studied traffic models for vehicular traffic as summarized in the overview articles on this topic [Hel01, BM00, NWW03, KW04]. The main purpose for these studies is to understand complex traffic flow phenomena and eventually to influence or even to control traffic flow.

There exist a large number of traffic flow models. A possible classification is to consider microscopic, kinetic and macroscopic models. In microscopic models the dynamics of the single drivers are described. Kinetic models mimic the Boltzmann equation in gas dynamics and deal with probability distributions. Finally, macroscopic models describe "macroscopic" quantities like traffic density and traffic flow velocity. Microscopic models have advantages from the modeling point of view whereas macroscopic models have their advantages in the simple description and the simulations. However, the study of the interesting (nonlinear) phenomena is highly challenging in all the modeling approaches. Here we focus on a widely studied class of microscopic models, the so-called follow-the-leader models.

A classical problem studied for microscopic models is the traffic dynamics on a circular road. Many interesting phenomena like the formation of *stop-and-go* waves can be observed in real experiments ([SFK$^+$08]). Some of the phenomena can be reproduced easily by simple microscopic models using periodic boundary conditions. Unfortunately, in many cases the nonlinear dynamics of a simple model is not studied carefully enough to encounter many or most of the dynamics of the model. Contrary to that, more and more complex models have been proposed. Our approach (already applied in the previous papers [GSW04, SGW09]) is to take very simple (nonlinear) microscopic traffic flow models and to study deeply the (nonlinear) dynamics of such a model. Surprisingly, we have learnt that already the very simple models show very rich dynamics which can be interpreted easily in the traffic flow context. A key point finding in the mathematical analysis of such simple models is bifurcations which lead to stable and unstable periodic solutions (in relative velocities and headways), coexisting multiple periodic and quasi-stationary solutions, etc. From a macroscopic viewpoint (considering the velocity and the inverse of the headway as the density) the quasi-stationary solutions are very simple constant velocity solutions, whereas the periodic solutions correspond to downstream traveling density and velocity waves. Moreover, the well-known inverse Greek Lambda structure in the flux-density (so-called fundamental) diagram diagram can be recovered.

The results mentioned above were mostly obtained for the circular road with identical or non-identical drivers. In the presence of a bottleneck (which could be due to roadwork on the circular road) the dynamics becomes even more interesting and the corresponding analysis changes dramatically. The reason for this is that the bottleneck-free case is very special and the resulting mathematical problem ends in a classical stability analysis for an equilibrium point of a system of autonomous ordinary differential equations (ODEs). This is not true anymore in the presence of a bottleneck. In [SGW09] a new mathematical approach for this problem was presented. With this approach new types of solutions were found. Macroscopically these new solutions correspond to standing (density and velocity) waves or to more complex interactions of traveling waves and standing waves. Mathematically these solutions are known rotational or quasi-rotational solutions. In the special case of identical drivers, they become the famous Ponies-on-a-Merry-Go-Round-solutions (POMs) (see [AGMP91]) or quasi-POMs.

In [SGW09] the main issue was to introduce this new approach for studying the dynamics in the case of bottleneck reducing the maximal velocity in a limited part of the circle. The reduction size of the maximal velocity is characterized by some parameter ε. Some simulations were presented to underline the potential of the method. However the main attention was given to the case of bottleneck with small ε . In this paper we focus on general (large) ε, which leads to new problems not only from the computational point of view. Our numerical investigation show that a bottleneck induces very interesting complex dynamics. We are able to classify some fundamental patterns (standing waves, traveling waves) and to identify more complex phenomena as combinations of these fundamental patterns. We note the interesting situation where we have different coexisting patterns. Depending on the initial data or on perturbations of the traffic situation one of these patterns is selected and appears. We mention that there are results about traffic phenomena induced by bottleneck based on a much more complex stochastic three-phase multi-lane theory in [Ker08]. We will comment on some analogies in section 3.

The paper is organized in the following way. In section 2 we summarize the existing results in this direction. In section 3 we present many new numerical results with interesting macroscopic visualizations showing discrete versions of the speed $v(\xi, t)$ as function of position ξ and time t. We give interpretations of the results in a traffic flow context. Finally we add a conclusion.

2. Theoretical setting. We study the situation of N cars on a circular road of length L. A widely used car following model describing such a situation is the well-known optimal velocity model introduced by Bando et al. [BHN$^+$95]. Here we use a generalization of the standard optimal velocity model. Let $x_j = x_j(t), t \geq 0$ be the distance the j-th car has covered at time t. Then the model reads

$$\ddot{x}_j = \frac{1}{\tau_j} \left(V_{j,\varepsilon}(\xi_j, x_{j+1} - x_j) - v_j \right), \quad j = 1, \ldots, N, \quad x_{N+1} = x_1 + L. \tag{2.1}$$

The circular road is represented by the fact that $x_{N+1} = x_1 + L$, i.e. the N-th car is following the first car. Then we have to explain the optimal velocity function $V_{j,\varepsilon}$. Let $V_j = V_j(d_j)$ be the optimal velocity function of the j-th car depending on the headway $d_j = x_{j+1} - x_j$ which is the distance between the j-th car and the $j+1$-th car in front. The optimal velocity function expresses the velocity the j-th car is aiming to achieve, according to the distance to the car in front. This function is assumed to

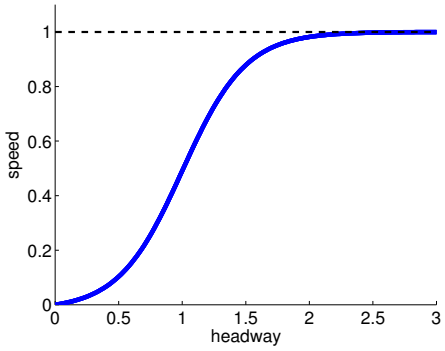

FIG. 2.1. *An example of an optimal velocity function*

be

$$
\begin{aligned}
V_j : [0,\infty) &\to [0,\infty), \qquad \text{smooth and strictly monotone increasing} \\
V_j(0) &= 0, \\
\lim_{d_j \to \infty} V_j(d_j) &= V_{j,max}.
\end{aligned} \tag{2.2}
$$

An example is given in Figure 2.1. In [SGW09], a bottleneck (caused for example by roadwork) was introduced by extending the optimal velocity function to

$$V_{j,\epsilon}(\xi, y) = \left(1 - \epsilon e^{-(\xi - \frac{L}{2})^2}\right) V_j(y). \tag{2.3}$$

The (position) variable ξ is defined by

$$0 \le \xi \le L, \qquad \xi = x \bmod L, \tag{2.4}$$

where x denotes a position and y a headway. The bottleneck is centered around the position $\xi = \frac{L}{2}$ and it acts by reducing the maximal velocity. The parameter $\epsilon \ge 0$ describes the "strength" of the bottleneck (see Figure 2.2). Model (2.1) says that every driver aims to reach his optimal velocity which depends on the headway and on the position with respect to the bottleneck.

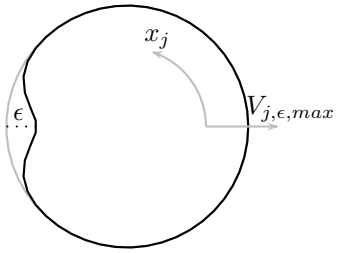

FIG. 2.2. *A region of reduced maximal optimal velocity* $V_{j,\epsilon,max}$.

In the last decade various simplified versions of this model have been studied. In the general case of non-identical drivers every single car obeys its own optimal velocity law. In the examples we study in section 3 identical drivers are assumed. We recall some results for the various versions of identical and non-identical drivers with and without bottleneck. An overview is given in Table 2.

	solution	bifurcation	solution due to bifurcation
identical and non-identical drivers, no bottleneck	quasi-stationary	Hopf	Hopf-periodic solution, traveling waves
non-identical drivers with bottleneck	rotation, standing wave	Neimark-Sacker	quasi-rotation, interacting standing and traveling waves
identical drivers with bottleneck	POM, standing wave	Neimark-Sacker	quasi-POM, interacting standing and traveling waves

TABLE 2.1
Overview on solutions and bifurcations

2.1. Non-identical drivers without bottleneck. We recall (2.1) in the case $\varepsilon = 0$ and write it as a first order (nonlinear) system

$$\left\{ \begin{array}{rcl} \dot{x}_j & = & v_j \\ \dot{v}_j & = & \frac{1}{\tau_j}(V_j(x_{j+1} - x_j) - v_j) \end{array} \right\}, \quad j = 1, \ldots, N, \quad x_{N+1} = x_1 + L. \tag{2.5}$$

Although this model – and especially the corresponding version with identical drivers in section 2.2 – is very simple it has become an important tool in the description of traffic flow on a circular road. This is due to the fact that there exist simple solutions – called *quasi-stationary solutions* – which can be observed in real experiments on a circular road setting [SFK+08]. Quasi-stationary solutions (with superscript 0) are given by

$$\begin{aligned} v_j^0(t) &= v^0 \\ x_j^0(t) &= x_1^0(0) + \sum_{k=1}^{j-1} d_k^0 + t\, v^0, \qquad j = 1, ..., N, \end{aligned} \tag{2.6}$$

where v^0 is the same (constant) velocity of all cars and d_k^0, $k = 1, .., N$ represent the (constant) headways satisfying

$$v^0 = V_j(d_j^0), \quad j = 1, .., N, \qquad \sum_{j=1}^{N} d_j^0 = L. \tag{2.7}$$

The terminology quasi-stationary solution is due to the fact that this solution itself is (obviously) not stationary, but the corresponding velocities v^0 and headways d_j^0 are. Even more, the velocities v^0 and headways d_j^0 are stationary solutions of the corresponding model for the relative velocities and the headways.

The question whether a quasi-stationary solution can be observed in reality or not is related to the stability as a solution of the nonlinear ODE system (2.5) with $2N$ equations. However, a related (linear) stability analysis is only possible in special cases (see [GSW04, GSSW07]).

2.2. Identical drivers without bottleneck. Now we assume that all drivers are identical, i.e. that the optimal velocity functions $V_j = V$, $j = 1, ..., N$ and the

relaxations times $\tau_j = \tau$, $j = 1, ..., N$, are equal for all cars. Again, the case $\varepsilon = 0$ stays for no bottleneck. Then we have

$$(2.8) \quad \left\{ \begin{array}{rcl} \dot{x}_j & = & v_j \\ \dot{v}_j & = & \frac{1}{\tau}(V(x_{j+1} - x_j) - v_j) \end{array} \right\}, \quad j = 1, \ldots, N, \quad x_{N+1} = x_1 + L.$$

In fact, this is the model presented originally by Bando et al [BHN$^+$95]. It was studied by various authors (see [GSW04] and references therein).

As already mentioned, this model has become an important tool in the description of traffic flow on a circular road. Many phenomena discovered in real experiments on a circular road setting [SFK$^+$08] can be described by the simple model (2.8). Since here $d_j^0 = d^0 = L/N$ for $j = 1, ..., N$, the quasi-stationary solutions are given by

$$(2.9) \qquad x_j^0(t) = (j-1)\frac{L}{N} + t\, V\Big(\frac{L}{N}\Big) + x_1^0(0), \qquad j = 1, ..., N.$$

Also, it is well-known from the literature that for our model the quasi-stationary solutions are asymptotically stable if $V'(\frac{L}{N}) < \frac{1}{1+\cos\frac{2\pi}{N}}$ (see [Hui02, GSW04]). When the parameters are such that the critical value $V'(\frac{L}{N}) = \frac{1}{1+\cos\frac{2\pi}{N}}$ is reached, then a qualitative change in the dynamics occurs. This is called a bifurcation. In the traffic context the critical parameter correspond to a critical mean density on the circular road. When the critical density is exceeded the simple quasi-stationary solutions cannot be observed any more. In our case a so called Hopf bifurcation occurs. A Hopf bifurcation generates periodic solutions for parameters close to the critical one (see [IIN$^+$01, GSW04] and [OWK04, OKW05] for delay models). These bifurcating periodic solutions which we will call *Hopf-periodic* are traveling waves showing the well-known oscillations in headway and velocity such that the congestion travels upstream (see Figure 3.4(b)). They can be observed in real experiments [SFK$^+$08] and are sometimes named as *stop-and-go* waves (even though in most of the Hopf-periodic solutions no real stop (vanishing velocity) appears). Therefore the Hopf-periodic solutions are a very important class of nontrivial solutions which can be observed in reality. Mathematically – by analyzing the related Lyapunov exponent – the stability of the Hopf-periodic solutions can be determined, too. In case of non-stationary solutions there are various definitions of stability. The one we are talking about here is the so called orbital stability.

However, the bifurcation results are of local type, valid only in a small neighborhood of the critical parameter values. Using special numerical tools (path following methods) one can study the global bifurcation diagram. Then many additional nontrivial (stable and unstable) periodic solutions can be found. Interesting phenomena like coexistence of multiple periodic and quasi-stationary solutions have been discovered. Details on the global bifurcation analysis can be found in [GSW04].

2.3. Non-identical drivers with bottleneck. In the case of bottleneck we use the general model (2.1) for non-identical drivers with optimal velocity function (2.3). Here quasi-stationary solutions of type (2.9) do not exist anymore and the standard tools are no more applicable. In other words, the situation in the previous sections 2.1 and 2.2 was mathematically very special since the quasi-stationary solutions formed a stationary point in the system for the relative velocities and the headways. Therefore standard methods for the stability analysis of stationary points of autonomous ODE systems could be applied. In the more general case with bottleneck the situation is different since we do not know what the generalization of a quasi-stationary solution

is. Rewriting the system in terms of relative velocities and headways does not show any advantage since there are no interesting stationary points. Therefore in this case a completely different approach has to be used. It turns out that so-called rotation solutions are the right object to look for (see [SGW09]).

A rotation solution with orbital period T and rotation number $k \in \mathbb{Z}$ of (2.1) is defined by

$$x_j(t+T) = x_j(t) + kL, \quad v_j(t+T) = v_j(t), \qquad j = 1, 2, ..., N, \tag{2.10}$$

where T and k are assumed to be minimal. We will restrict to the special, but most important case $k = 1$. From a traffic point of view a rotation solution is nothing but a standing wave for the velocity or the headways (see Figure 3.3).

We see that for $\varepsilon = 0$, our quasi-stationary solutions are (trivial) rotation solutions with *orbital period* $T := L/v^0$, where v^0 is the common velocity of the drivers. But observe that the Hopf-periodic solutions (traveling waves) in general are *not* rotation solutions with orbital period T. They always satisfy

$$x_j(t+T) = x_j(t) + L_p, j = 1, 2, ..., N \tag{2.11}$$

with an orbital length L_p. If L_p and L are commensurate, formally the Hopf-periodic solutions are rotation solutions with possibly large orbital periods and rotation numbers k.

Now we rewrite our problem in a fixed point problem. The time-T-map Φ^T is defined as follows: Assume that $\mathbf{x}(0) = (x_1, ..., x_N, v_1, ..., v_N)$ is the state of our system at time $t = 0$ and that $\mathbf{x}(t)$ is the solution of the corresponding initial value problem. Then

$$\Phi^T(\mathbf{x}(0)) = \mathbf{x}(T). \tag{2.12}$$

Setting $\mathbf{\Lambda} := (L, ..., L, 0, ..., 0)$, rotation solutions ($k = 1$) satisfy (rewriting (2.10))

$$\Phi^T(\mathbf{x}(t)) = \mathbf{x}(t+T) = \mathbf{x}(t) + \mathbf{\Lambda} \text{ for all } t. \tag{2.13}$$

Therefore, rotation solutions are fixed points of the map Q defined by

$$Q(\mathbf{x}) = \Phi^T(\mathbf{x}) - \mathbf{\Lambda}. \tag{2.14}$$

This means that in case of bottleneck instead of quasi-stationary solution we have rotation solutions solving the fixed point problem (2.14). Note that when looking for rotation solutions we do not know the period T a priori. For mathematically interested readers we mention that we will not consider the map Q itself, but a related Poincaré map Π. A Poincaré map looks for discrete times whenever the car number 1 passes the position $\xi = 0$ (we could take also any other position and any other car).

Again, the question whether a solution can be observed in real traffic situations or in experiments is related to the stability of the solution. The corresponding stability concept for rotation solutions was discussed in [SGW09]. We note that – similar to the bottleneck-free case – when reaching a critical density the rotation solutions may loose their stability. This is due to another type of bifurcation, a so called Neimark–Sacker bifurcation. In the bottleneck-free case – when passing the critical parameter values – Hopf-periodic solutions bifurcate whereas Neimark-Sacker bifurcation leads so called quasi-rotation solutions. We will see that contrary to Hopf-periodic or rotations

solutions is not so easy to identify quasi-rotation solutions. We will see that they seem to be combinations of standing and traveling waves.

As a consequence, in the (L, ϵ)-plane we conjecture parameter regions where rotations and quasi rotations exist which at $\epsilon = 0$ coincide with the quasi-stationary solutions and the Hopf-periodic solutions, respectively. Between these two parameter regions we expect a curve on which Neimark–Sacker bifurcations take place for $\epsilon > 0$. At Hopf values L^H such a curve will emanate at $(0, L^H)$. In fact, in section 3 we will extensively study different parameter regions to verify this conjecture (see Fig. 3.2).

In [SGW09] we showed the existence of rotation solutions for small $\varepsilon > 0$ by considering the case of a small bottleneck as a perturbation of the bottleneck-free case. Hopf-periodic solutions are perturbed to quasi-rotations.

2.4. Identical drivers with bottleneck. We restrict and simplify the setting to the case of identical drivers. This is done by adding an additional symmetry condition to a rotation solution, namely

$$x_j(t + T/N) = x_{j+1}(t) \text{ for all } t, \quad j = 1, 2, ..., N. \tag{2.15}$$

This means that in the case of identical drivers all cars behave in the same way except a time shift of T/N between two cars. Rotation solutions satisfying (2.15) are known as Ponies-on-a-Merry-Go-Round-solutions (POMs) (see [AGMP91, SGW09]). It turns out that the method to search rotation solutions presented in the previous section 2.3 can be simplified considerably. The additional condition (2.15) allows the use of so-called reduced Poincaré maps π, and the computation of POMs can be based on π in a very efficient way. While the Poincaré map looks for discrete times whenever the car number 1 passes the position $\xi = 0$, the reduced Poincaré map lists the whole configuration at discrete times whenever any car passes the position $\xi = 0$. This gives a denser discrete time grid on which the dynamics is evaluated.

Mathematically, POMs correspond to fixed points and quasi-POMs to invariant curves of π which bifurcate in Neimark–Sacker-points of π. Again, quasi-stationary solutions correspond to POMs and Hopf-periodic solutions to quasi-POMs for $\varepsilon = 0$.

Our numerical analysis in the following section 3 is performed for the model of identical drivers and is based on the use of reduced Poincaré maps. More theoretical details can be found in [SGW09].

2.5. Traffic flow and "Flocking". Here we point out the following alternative viewpoint of the dynamics of the microscopic traffic flow models. The single drivers can be seen as individual self-propelled agents. Each agent follows simple rules which in our case involve only the agent (driver) in front. The dynamics we observe is the result of the collective motion of all the individual agents. There is no central control of the dynamics. In the case of (asymptotically) stable quasi-stationary solutions all agents (drivers) tend to the same asymptotic velocity. For a stable POM solution all drivers approach the same velocity profile (at least for somehow "close" initial profiles). In population dynamics this phenomenon is referred as "flocking" (or "herding" etc.). For more details see [CS07]. In this sense on the circular road we can observe a one dimensional version of "flocking".

3. Numerical results. We consider the general model (2.1) for identical drivers,

$$\left.\begin{array}{rcl} \dot{x}_j &=& v_j \\ \dot{v}_j &=& \frac{1}{\tau}(V_\varepsilon(\xi_j, x_{j+1} - x_j) - v_j) \end{array}\right\}, \quad j = 1, \ldots, N, \quad x_{N+1} = x_1 + L. \tag{3.1}$$

with

$$V_\epsilon(\xi, y) = \left(1 - \epsilon e^{-(\xi - \frac{L}{2})^2}\right) V(y). \tag{3.2}$$

We restrict our attention to $N = 10, \tau = 1$ and to the Bando optimal velocity function

$$V(y) = v_{max} \frac{\tanh a(y-1) + \tanh a}{1 + \tanh a} \tag{3.3}$$

with $a = 2, v_{max} = 1$.

We know that for $\varepsilon = 0$ there exist two Hopf bifurcation points with respect to L, namely $L_1^H = 5.890$ and $L_2^H = 14.109$. The larger value L_2^H is more interesting, since it is connected with the first loss of stability of the quasi-stationary solutions for increasing traffic densities N/L. Moreover, we know that the quasi-stationary solutions (being special POMs) are unstable for $L_1^H < L < L_2^H$.

It is impossible to give a complete survey about the dynamics of the model for all parameter pairs (L, ε). We will mainly present some results for two fixed values of L, namely $L = 13 < L_2^H$ and $L = 18 > L_2^H$.

The dynamics of POMs and quasi-POMs will be visualized in three ways using suitable projections.

1. Speed of a single car as a function of length (Lagrangian description). For a POM we will encounter an L-periodic pattern (example: Figure 3.3(a)).
2. Macroscopic view (Eulerian description). This is obtained by coloring all trajectories according to the speed of the corresponding car. Hereby we obtain a discrete version of the speed $v(\xi, t)$ as function of position ξ and time t. One single trajectory is drawn (example: Figure 3.3(b)).
   For a POM, $v(\xi, t)$ is independent of t. For a quasi-POM we have the interesting observation that $v(\xi, t)$ is periodic in t. However, this observation is still without proof.
3. More mathematically, the orbit under the reduced Poincaré map, mainly showing the limit set. For a POM the limit set is just a point, for a quasi-POM we will encounter closed invariant curves (example: Figure 3.7(a)).

3.1. POMs (standing waves). We are interested in how the POMs change with ε for fixed L. To this end we continue numerically POM-branches in dependence on (as a function of) the bottleneck strength ε using the characterization of POMs as fixed points of (reduced) Poincaré maps. .

From the theory in [SGW09] we know that for fixed L, a POM-branch parametrized by $\varepsilon \geq 0$ emanates from the quasi-stationary solution ($\varepsilon = 0$). We will path follow POM-branches also for larger values of ε. Some results are visualized in Fig. 3.1. As expected we encounter Neimark–Sacker bifurcation points, but also – less expected – folds.

In Fig. 3.1 (vertical axis) a POM is characterized by the average speed $v_M := L/T$ with T being the orbital period. v_M is proportional to the space-averaged flow. The horizontal coordinate is the bottleneck strength ε. For $\varepsilon = 0$ the trivial POM coincides with the quasi-stationary solution where all cars have the same speed $v_M = V(L/N)$. The numerical continuation is not influenced by the stability of the POMs. Of an obvious interest are those (bifurcation) parameters ε where stability is lost or gained. We encounter two qualitatively different bifurcations: Neimark-Sacker points (as in Fig. 3.1(a) denoted by N) and fold points (as in Fig. 3.1(d) denoted by F_1 and F_2).

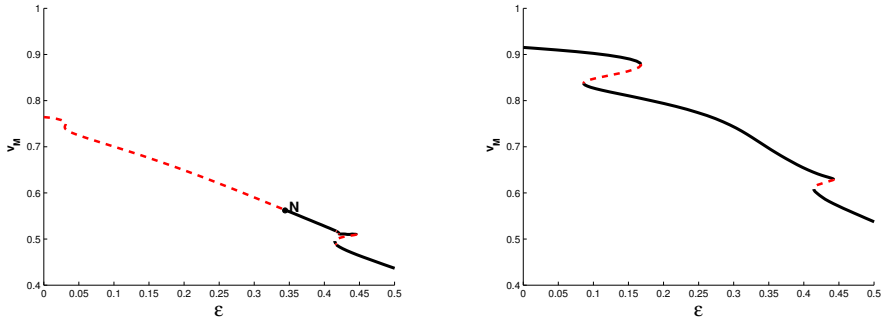

(a) $L = 13$ (b) $L = 16$

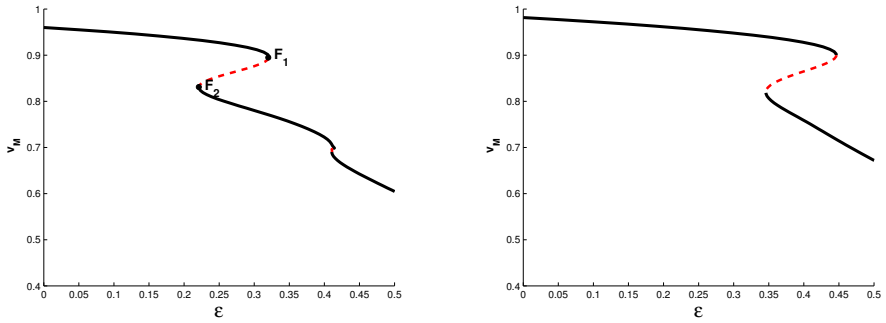

(c) $L = 18$ (d) $L = 20$

FIG. 3.1. $N = 10$. *Dependence of the average speed v_M of the POMs on ε for fixed L. Solid (dashed) lines: Stable (unstable) POMs. The Neimark-Sacker bifurcation in (a) is indicated by the letter N. Folds in (c) are indicated by the letters F_1 and F_2.*

In Figure 3.1 folds can be found on the POM-branches. For $L = 18$ there are two folds for $\varepsilon_1 := 0.22$ and for $\varepsilon_2 := 0.313$, two other folds are very close together at $\varepsilon \approx 0.41$. Observe that the S-shape of the POM-branch with two neighbored folds are associated with the coexistence of two stable POMs for the same parameter set. We will see that the wave-speed of these two stable POMs in the vicinity of the bottleneck differs significantly. This is already indicated by the corresponding different average speeds.In the mentioned theory of Kerner [Ker08] the POMs seem to correspond to the so called congested traffic phase.

3.1.1. Bifurcation diagrams in L and ε. A bifurcation diagram in a parameter plane shows bifurcation curves. By this it contributes to the information about possible dynamics for a fixed pair of parameters.

In our traffic model we expect Neimark–Sacker and fold curves showing the dependence of the bifurcation parameters ε on the circle length L. Figure 3.2 contains Neimark–Sacker (red) and fold curves (black) in the (L, ε)-parameter plane. The Neimark-Sacker curve emanates in the Hopf point $(0, L_2^H)$.

Though these curves deliver only local information, we guess, supported by numerical simulations, that quasi-POMs live in the red-shaded region, where POMs are unstable. In the other parameter domains we expect stable POMs. In the black-shaded areas, due to the S-shape of the POM-branches in Figure 3.1, we expect two stable POMs and one unstable POM.

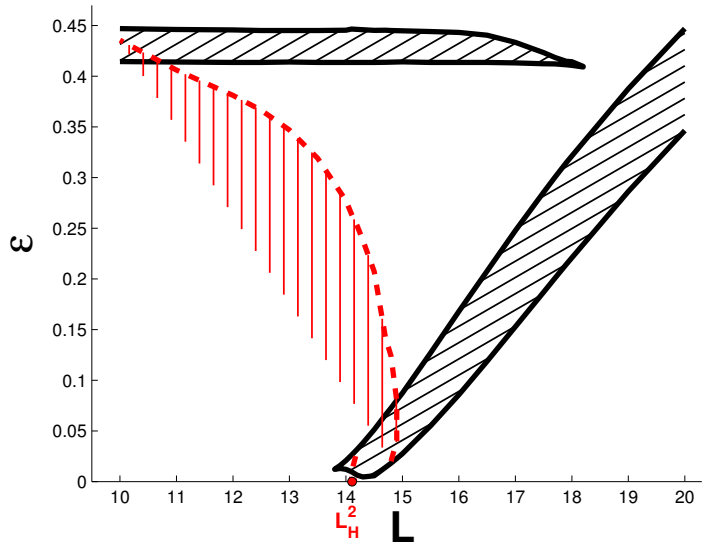

FIG. 3.2. $N = 10$. *Bifurcation diagram. Neimark-Sacker curve (red, dashed line), fold curves (black, solid line*

3.1.2. POMs for L=18. Figure 3.3 visualizes different stable POMs for $L = 18$ and various ε-values. They can be computed directly by Newtons method as fixed points of the reduced Poincaré maps — in contrast to the quasi-POMs which we get only by simulation, see Section 3.2. From Figure 3.1(c) we conclude, that for some values ε, the corresponding POMs are not unique. For example, there are two coexisting stable POMs and one unstable POM for $\varepsilon = 0.3$, a value between the two fold values $\varepsilon_1 = 0.22$ and $\varepsilon_2 = 0.313$, see Figures 3.3(c) - 3.3(f). These two stable POMs are qualitatively very different. This is already indicated by the difference of their average speeds v_M.

Remarkably, the decrease of speed induced by the bottleneck is considerably large only for the POMs in the last two rows of Figure 3.3. Here traffic jams occur downstream the bottleneck while for the POMS in the first two rows of Figure 3.3 the minimal speed occurs upstream the bottleneck (the black circles in Figure 3.3). For $\varepsilon = 0.3$ both types of stable POMs do exist.

3.2. Quasi-POMs for L=13. In this section we fix $L = 13$. We know from Figure 3.2 and particularly from Figure 3.1(a) that there is a wide parameter range where POMs emanating from the quasi-stationary solutions for $\varepsilon = 0$ are unstable. Here we expect quasi-POMs.

We present three different visualizations of quasi-POMs, see Figures 3.4-3.7. Again each quasi-POM is associated with the average speed v_M where the average is taken over a suitable large time interval.

Quasi-POMs are special solutions which show non-periodic dynamic behavior for $t \to \infty$ when considering the trajectories of individual vehicles. Theoretically, the quasi-POM type irregularity can be identified by closed invariant curves of (reduced) Poincaré maps as shown in Figure 3.7. But we found another way of identification, namely the time-periodicity of the macroscopic function $v(\xi, t)$ in the macroscopic

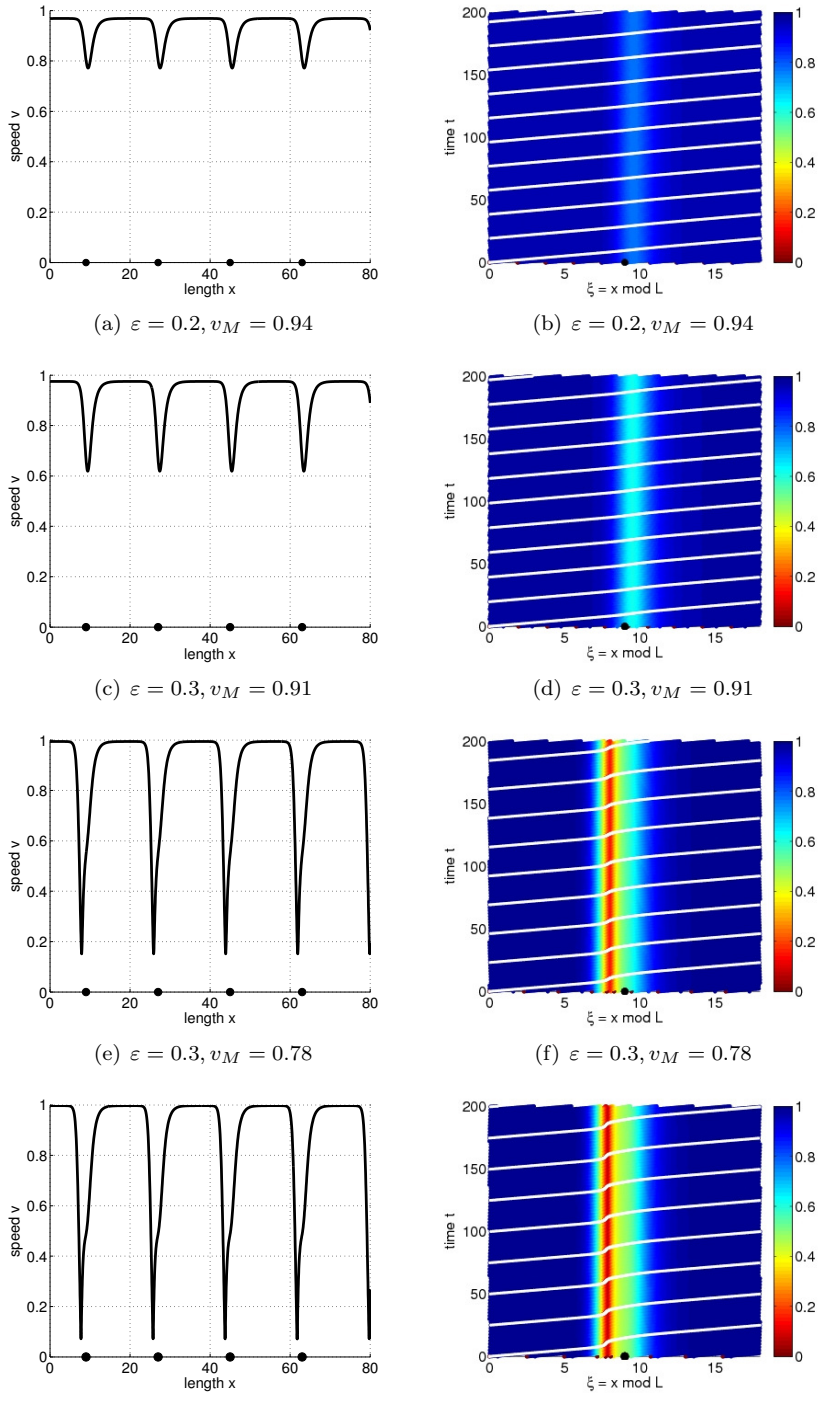

(a) $\varepsilon = 0.2, v_M = 0.94$ (b) $\varepsilon = 0.2, v_M = 0.94$

(c) $\varepsilon = 0.3, v_M = 0.91$ (d) $\varepsilon = 0.3, v_M = 0.91$

(e) $\varepsilon = 0.3, v_M = 0.78$ (f) $\varepsilon = 0.3, v_M = 0.78$

(g) $\varepsilon = 0.4, v_M = 0.72$ (h) $\varepsilon = 0.4, v_M = 0.72$

FIG. 3.3. $N = 10$. *Stable POMs for* $L = 18$ *and different* ε*: Speed versus length (left) and macroscopic view (right) with a trajectory of a single car in white. The position of the bottleneck and its size (right) are indicated by black circles. Note that for* $\varepsilon = 0.3$ *there are two different stable POMs.*

views in Figures 3.4-3.6 (right side).

In Figure 3.1(a) there is a Neimark–Sacker bifurcation for $\varepsilon \approx \varepsilon_N := 0.347$, and the POMs are stable for $\varepsilon > \varepsilon_N$ and unstable for $\varepsilon < \varepsilon_N$. Hence one could expect quasi-POMs for $\varepsilon < \varepsilon_N$.

Moreover, we know that for $\varepsilon = 0$ the quasi-stationary solution is unstable. The Hopf point at L_2^H is responsible for the occurrence of a stable headway- and speed-periodic solution appearing as a traveling wave. In our new context (see sec. 2) this solution is a quasi-POM. Its traveling wave dynamics is visualized in Figure 3.4(a) and Figure 3.4(b). The corresponding invariant curve can be seen in Figure 3.7(a). We expect that this special quasi-POM for $\varepsilon = 0$ is perturbed to quasi-POMs for $\varepsilon > 0$.

Indeed, for various values of ε with $0 < \varepsilon < \varepsilon_N$ we found quasi-POMs by simulation. Figures 3.4-3.6 show how the macroscopic speed-pattern is changed due to increasing ε from $\varepsilon = 0$ (traveling wave) to $\varepsilon = 0.35$ (POM). There is an interaction of the traveling wave with the bottleneck. For $\varepsilon \in [0, 0.24]$ the traveling wave structure of the Hopf-periodic wave persists. For larger bottleneck strength ($\varepsilon \geq 0.25$) the traveling wave structure does not exist anymore. There appears more than one congestion upstream the bottleneck and a rather free-flowing traffic downstream.

Similar to POMs for $L = 18$, a coexistence of two different stable dynamics was found for $L = 13$. Looking more thoroughly on the last two rows in Figure 3.6 we see that there is a coexistence of two qualitatively different quasi-POMs for $\varepsilon = 0.25$, one of which – the second – seems to be the "Neimark–Sacker-successor" of quasi-POMs emanating in ε_N, the other the "Hopf-successor" of quasi-POMs emanating in $\varepsilon = 0$. One should also compare the corresponding invariant curves in Figure 3.7(c) and Figure 3.7(d). The quasi-POM visualized in Figure 3.7(d) seems to have less dramatic dynamics since the headways are farther away from zero than that in Figure 3.7(c). On the other hand, this quasi-POM has a slightly less average speed v_M than the other. Obviously, in Figure 3.5(d) on each round a car trajectory (in white) in general passes two congestions uptream the bottleneck while the trajcetory in Figure 3.5(b) crosses only one jam area (dark red) in each round which is in general "stronger" than the jam areas in Figure 3.4.

Again, let us mention a possible analogy to the theory of Kerner [Ker08]. The quasi-POMs with traveling wave character in Figure 3.4 seem to be realizations of the so called jam phase whereas the "fixed" (at the bottleneck) quasi-POMs in Figure 3.5(c,d) and 3.6 make part of the congested phase. A possible passage from a "fixed" quasi-POM to a traveling wave quasi-POM (by changing the density) would correspond to the so called pinch effect in the Kerner theory. However let us underline that the results of Kerner are based on much more complex stochastic multi-phase and multi-lane theory.

3.2.1. Invariant curves. To analyze the type of irregularity of a certain dynamics one has to look at the orbit of the (reduced) Poincaré map. If the limit set of the orbit is a closed invariant curve, we have the dynamics of a quasi-POM. A Neimark–Sacker bifurcation leads to such bifurcating invariant curves. Figure 3.7 shows projections of the invariant curves on the speed-headway plane of the fourth car, counted from the observation place at the measure point ($\xi = 0$). Since there are $N = 10$ cars, we expect that the 4th car is rather close to the center of the bottleneck having hence a more interesting dynamics than cars far away.

There is still no powerful numerical tool to continue invariant curves of quasi-POMs as a function of parameters. If this would be available, we guess that there

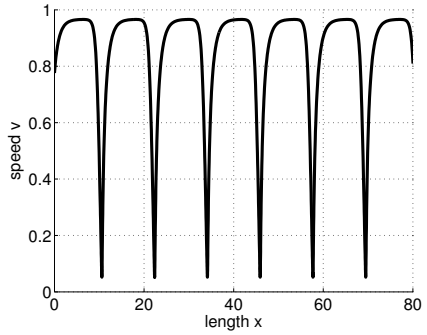

(a) Hopf-periodic dynamics. $\varepsilon = 0, v_M = 0.67$

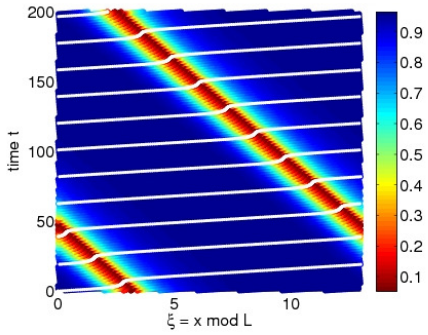

(b) Macro view of (a). $\varepsilon = 0, v_M = 0.67$

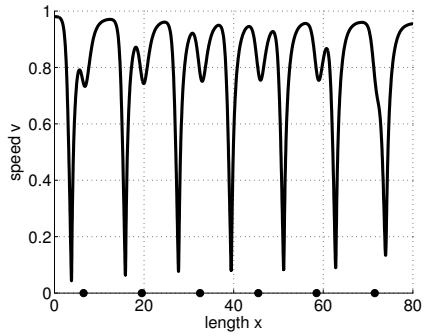

(c) $\varepsilon = 0.2, v_M = 0.65$

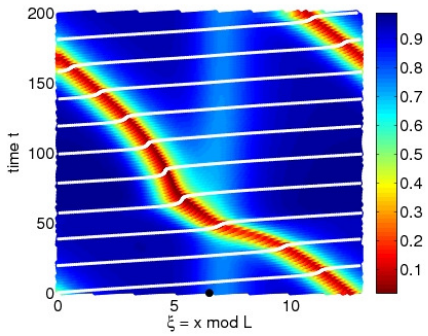

(d) $\varepsilon = 0.2, v_M = 0.65$

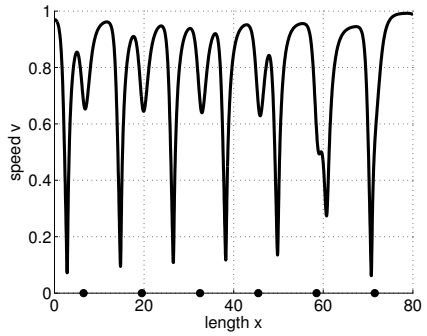

(e) $\varepsilon = 0.24, v_M = 0.65$

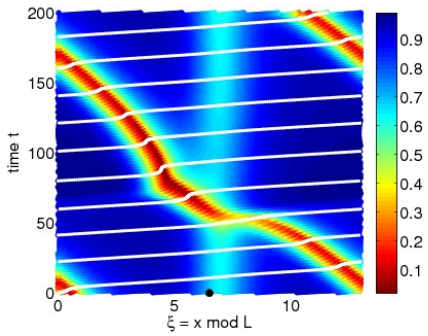

(f) $\varepsilon = 0.24, v_M = 0.65$

FIG. 3.4. $N = 10, L = 13$. *Quasi-POMs and their average speeds* v_M *for* $0 \le \varepsilon \le 0.25$*: Speed versus length (left) and macroscopic views (right). The position of the bottleneck is indicated by black circles.*

might be a S-shaped branch of quasi-POMs with respect to ε connecting the quasi-POMs of Neimark–Sacker type and that of Hopf-type and possessing two folds near $\varepsilon = 0.25$.

3.3. Other values of L. Up to now we have chosen mainly $L = 13$ and $L = 18$ and $0 \le \varepsilon \le 0.5$. Our dynamical simulations yielded POMs and quasi-POMs, nothing else. This is different for smaller values of L where we guess more complex dynamics.

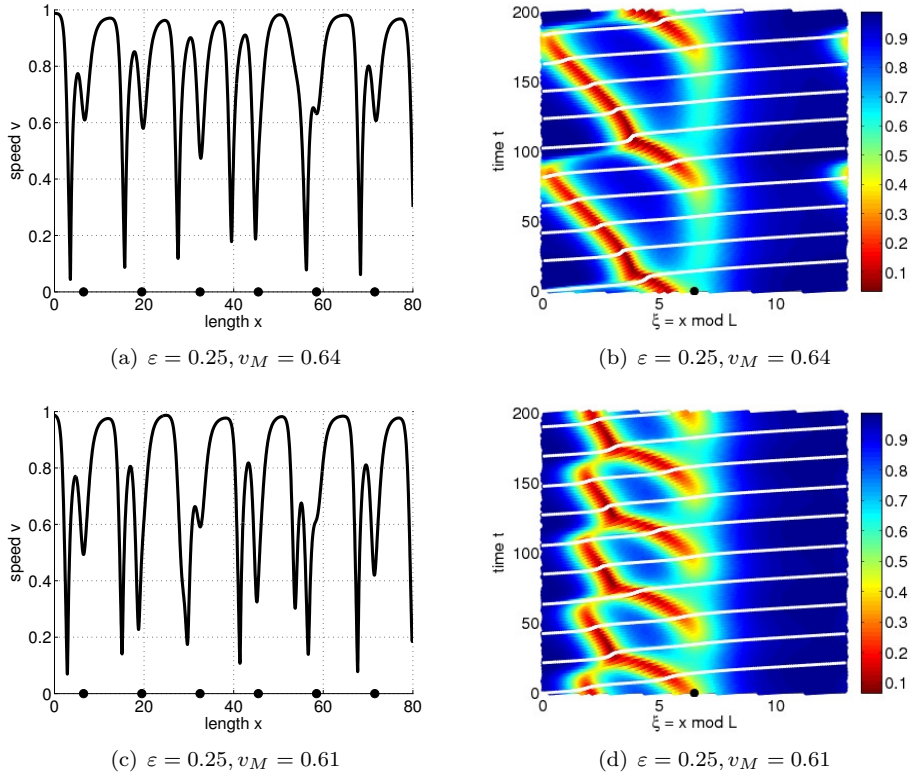

(a) $\varepsilon = 0.25, v_M = 0.64$ (b) $\varepsilon = 0.25, v_M = 0.64$

(c) $\varepsilon = 0.25, v_M = 0.61$ (d) $\varepsilon = 0.25, v_M = 0.61$

FIG. 3.5. $N = 10, L = 13$, *quasi-POMs. Continuation of Fig. 3.4. Coexistence of two different quasi-POMs for* $\varepsilon = 0.25$.

Figure 3.8(a) shows a chaotic like pattern for $L = 8$ — no time-periodicity is observed. Figure 3.8(b) shows a quasi-POM which may be due to a period-doubling process in increasing ε from $\varepsilon = 0$ to $\varepsilon = 0.3$ for $L = 10$.

3.4. Fundamental diagrams. Studying fundamental diagrams (i.e. flux-density-diagrams) in a microscopic optimal velocity models seems to be an uninteresting topic. The main input in the model is the optimal velocity function and we may expect a density flow relation according to the optimal velocity function.

Now we mimic a traffic-measurement by performing numerical simulations. We fix a measurement position $\xi = 0$ on the circular road and whenever a car passes this measurement position we take its velocity and the inverse of the headway (as approximation for the traffic-density). Note that our measurement position is on the opposite side of the bottleneck on the circular road. Since in a fundamental diagram we have to vary the density we perform the same measurement by varying the length L of the circular road (and keeping fixed the number of cars).

Suppose the dynamics on the circular road with identical drivers and no bottleneck corresponds to a quasi-stationary solution (constant headway $d^0 = L/N$ and constant velocity $v^0 = V(d^0)$). Let us denote the corresponding density by $\varrho^0 = \frac{1}{d^0}$. Then the corresponding flux $f^0 = f^0(\varrho^0)$ is given by the optimal velocity function

$$f^0(\varrho^0) = \varrho^0 \, V(\frac{1}{\varrho^0}). \tag{3.4}$$

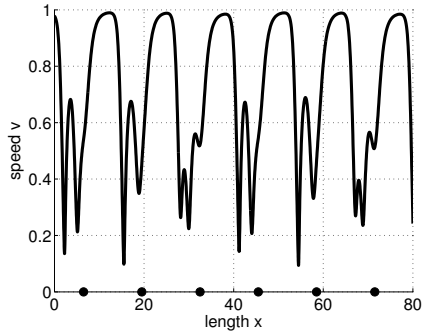

(a) $\varepsilon = 0.3, v_M = 0.59$

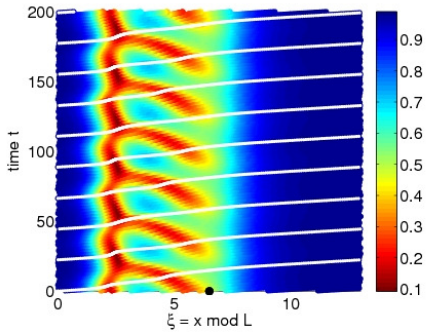

(b) $\varepsilon = 0.3, v_M = 0.59$

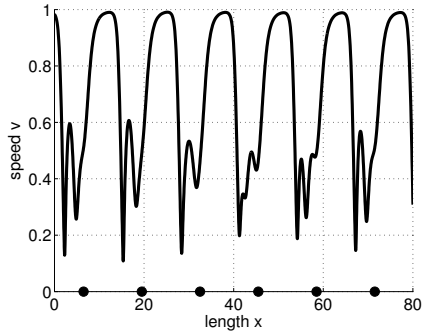

(c) $\varepsilon = 0.33, v_M = 0.57$

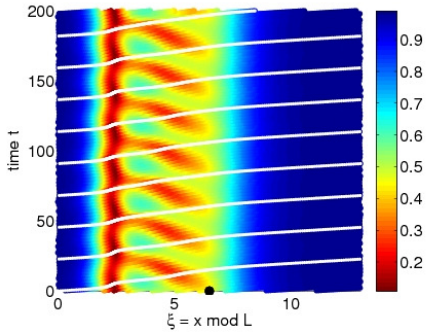

(d) $\varepsilon = 0.33, v_M = 0.56$

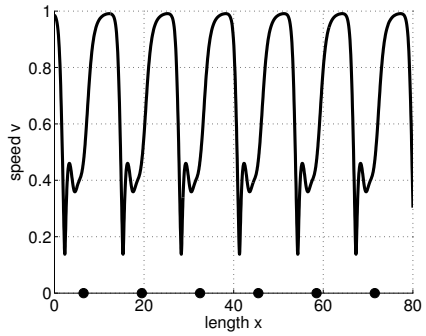

(e) POM for $\varepsilon = 0.35$. $v_M = 0.56$

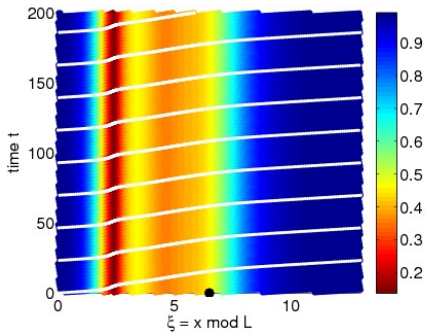

(f) POM for $\varepsilon = 0.35$. $v_M = 0.56$

FIG. 3.6. $N = 10, L = 13$, *(quasi-)POMs. Continuation of Fig. 3.5.*

This corresponds to the well known flux-density curves similar to the red curves in Figure 3.9.

However, this is only true for quasi-stationary solutions in the case of identical drivers with no bottleneck. In the bottleneck-free case we know that the quasi-stationary solution is unstable in a certain density interval. We know that in the unstable density interval the dynamics is driven by a Hopf-periodic solution and the measurement data will not lie on the red curves. In fact, in [SGW09] we showed that in general we recover the famous inverted Greek Lambda structure in the flux-density-

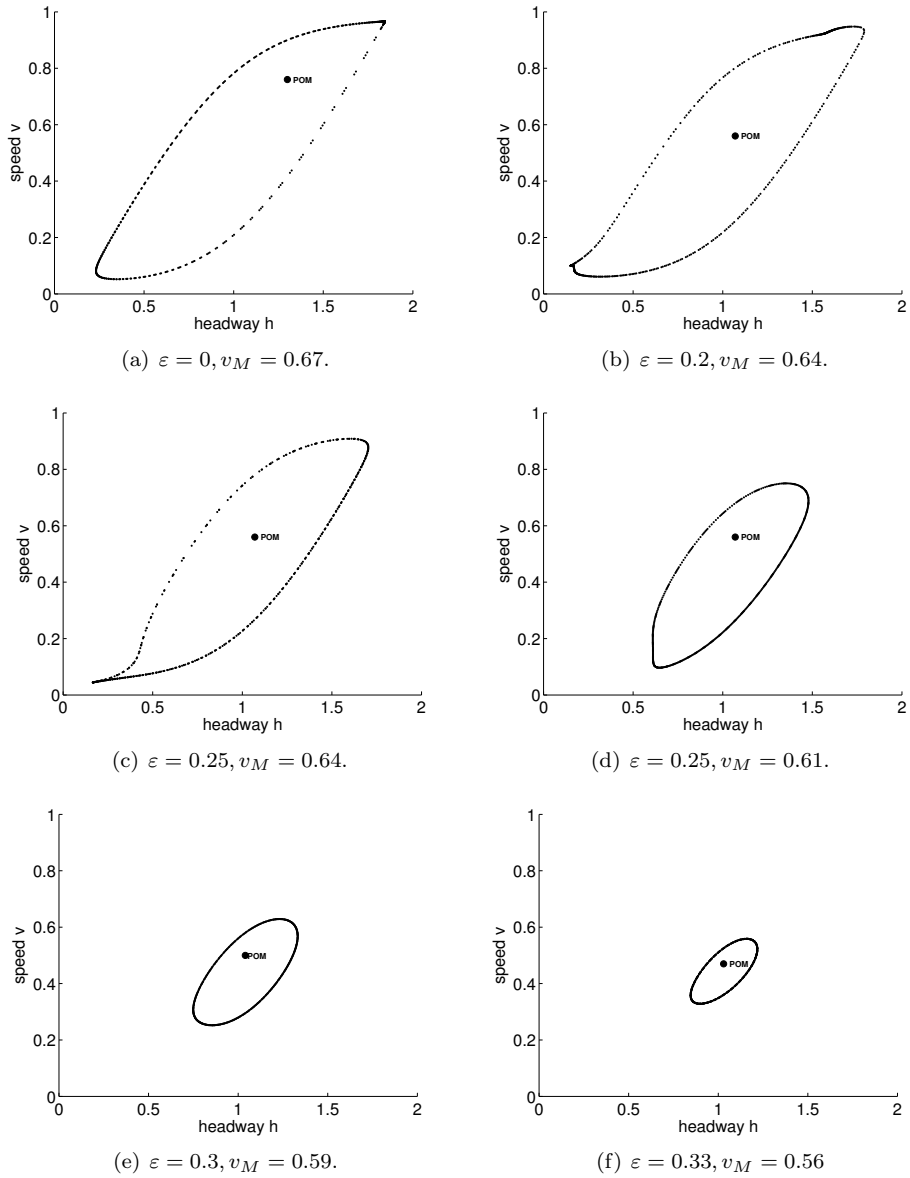

(a) $\varepsilon = 0, v_M = 0.67$.

(b) $\varepsilon = 0.2, v_M = 0.64$.

(c) $\varepsilon = 0.25, v_M = 0.64$.

(d) $\varepsilon = 0.25, v_M = 0.61$.

(e) $\varepsilon = 0.3, v_M = 0.59$.

(f) $\varepsilon = 0.33, v_M = 0.56$

FIG. 3.7. $N = 10, L = 13, 0.3 \leq \varepsilon \leq 0.33$. *Visualization of quasi-POMs in Figures 3.4-3.6 by invariant curves of the reduced Poincaré map for car No. 4,* $L = 13$ *and different values of* ε. *The unstable POMs are marked.*

diagram .

Here we study the flow-density diagrams for the case of (strong) bottleneck. In case of identical drivers we expect POM solutions (instead of quasi-stationary solutions). Those POMs are stable in a certain density region. Since POMs are standing waves and we measure at a fixed position on the circular road the resulting curve is very similar to the curves obtained for identical drivers with no bottleneck (quasi-stationary solution). The POMs are the red curves in the flux-density-diagram in

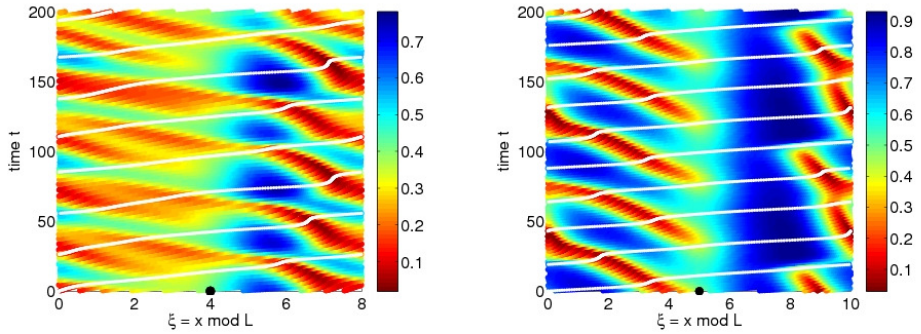

(a) $L = 8, \varepsilon = 0.4, v_M = 0.28$. Chaos?

(b) $L = 10, \varepsilon = 0.3, v_M = 0.45$: Quasi-POM. Result of period doubling ?

FIG. 3.8. $N = 10$. *Macroscopic visualization of two complex dynamics for* $L = 8$ *and* $L = 10$

Figure 3.9. In general the dynamics also involves quasi-POMs. The corresponding flux-density diagram becomes more complicated. In Figure 3.9 possible results for different values of ε are presented. We see that the resulting structures have partly lost their similarity to the inverse Greek Lambda. The complex dynamics involved in this simulations shows us that the resulting flux-density diagrams are not easy to interpret. We conclude that only in case of simple dynamics measurements result in known structures of the fundamental diagram.

4. Conclusions. In this paper we study traffic dynamics on a circular road with a bottleneck. For this setting in [SGW09] a new mathematical approach was presented. This approach enables to classify complex traffic dynamics on the circular road and therefore to improve the understanding of complex phenomena.

We are now able to interpret phenomena in case of bottleneck using analogies to the bottleneck-free case. This leads to traveling waves, standing waves and interactions of those two wave types which can be interpreted in the traffic flow context. Also coexisting stable patterns were observed in certain parameter regimes. The macroscopic viewpoint on the microscopic results helps considerably to interpret the dynamics.

We believe that this phenomenon persists for traffic models on the line. We made the interesting observation that quasi-POMs correspond to macroscopic functions $v(\xi, t)$ which are periodic in t. This is very helpful when classifying solution patterns. We will prove this conjecture in a forthcoming paper.

Acknowledgements. The first author is partially supported by the Marie Curie Early Stage Research Program DEASE (Differential Equations with Applications in Science and Engineering) of the European Union's 6th Framework Programme (Contract no. DEASE: MEST-CT-2005-021122).

We thank the two reviewers for their very valuable comments which helped to improve the paper considerably.

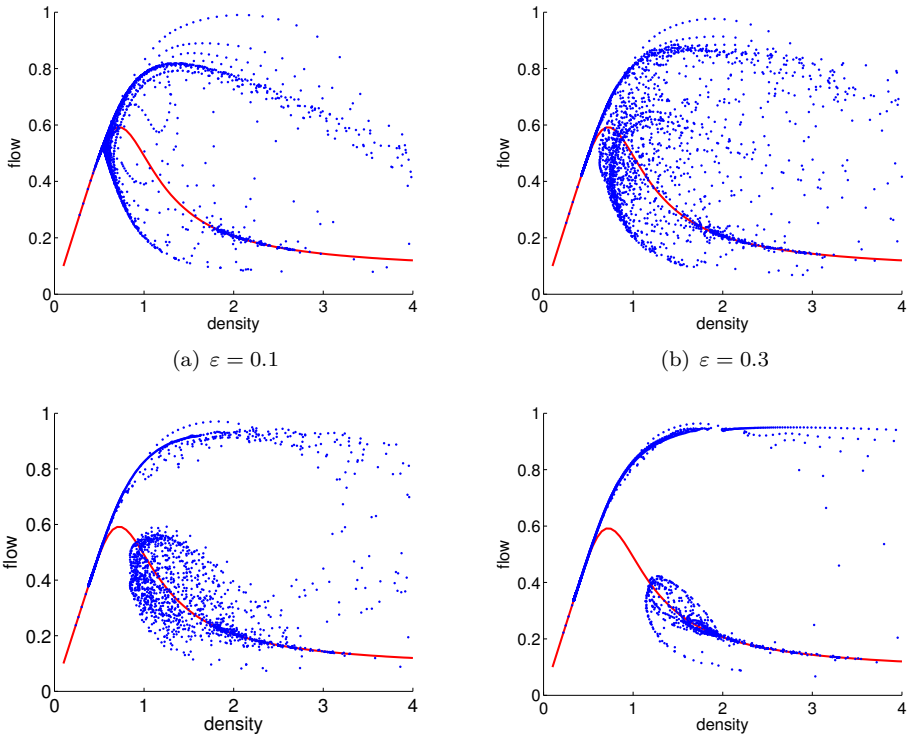

(a) $\varepsilon = 0.1$ (b) $\varepsilon = 0.3$

(c) $\varepsilon = 0.4$ (d) $\varepsilon = 0.5$

FIG. 3.9. *Fundamental diagrams for* $N = 10$ *and* $L = 4...20$ *at the measure point* $\xi = 0$. *Flow-density curve for the quasi-stationary solutions (red)*

REFERENCES

[AGMP91] D. G. Aronson, M. Golubitsky, and J. Mallet-Paret. Ponies on a merry-go-round in large arrays of josephson junctions. *Nonlinearity*, 4:903–910, 1991.

[BHN+95] M. Bando, K. Hasebe, A. Nakayama, A. Shibata, and Y. Sugiyama. Dynamical model of traffic congestion and numerical simulation. *Phys. Rev. E*, 51:1035–1042, 1995.

[BM00] M. Brackstone and M. McDonald. Car following: a historical review. *Transp. Res. F*, 2:181, 2000.

[CS07] F. Cucker and S. Smale. On the mathematics of emergence. *Japan J. Math.*, 2:197–227, 2007.

[GSSW07] I. Gasser, T. Seidel, G. Sirito, and B. Werner. Bifurcation analysis of a class of 'car following' traffic models ii: Variable reaction times and aggressive drivers. *Bulletin of the Institute of Mathematics, Academia Sinica*, 2(2):587–607, 2007.

[GSW04] I. Gasser, G. Sirito, and B. Werner. Bifurcation analysis of a class of 'car following' traffic models. *Physica D*, 197 (3-4):222–241, 2004.

[Hel01] D. Helbing. Traffic and related self-driven many-particle systems. *Rev. Modern Phys.*, 73:1067–1141, 2001.

[Hui02] H. J. C. Huijberts. Improved stability bound for steady state flow in a car-following model of road traffic in a circular road. *Phys.Rev. E*, 65:047103, 2002.

[IIN+01] Y. Igarashi, K. Itoh, K. Nakanishi, K. Ogura, and Yokokawa. Bifurcation phenomena in optimal velocity model for traffic flow. *Phys. Rev. E*, 64:047102, 2001.

[Ker08] B.S. Kerner. A theory of traffic congestion at heavy bottlenecks. *J.Phys. A: Math. Theor.*, 41:215101, 2008.

[KW04] A. Klar and R. Wegener. *Traffic flow: models and numerics.* Birkhaeuser, 2004. Editors: P. Degond, L. Pareschi, G. Russo.

[NWW03] K. Nagel, P. Wagner, and R. Woesler. Still flowing: approaches to traffic flow and traffic jam modeling. *Operations Research*, 51(5):681–710, 2003.

[OKW05] G. Orosz, B. Krauskopf, and R. E. Wilson. Bifurcations and multiple traffic jams in a car-following model with reaction-time delay. *Physica D*, 211:277–293, 2005.

[OWK04] G. Orosz, R. E. Wilson, and B. Krauskopf. Global bifurcation investigation of an optimal velocity traffic model with driver reaction time. *Phys. Rev. E*, 70:026207, 2004.

[SFK+08] Y. Sugiyama, M. Fukui, M. Kikuchi, K. Hasebe, A. Nakayama, K. Nishinari, S. Tadaki, and S.Yukawa. Traffic jams without bottlenecksexperimental evidence for the physical mechanism of the formation of a jam. *New J. Phys.*, 10:033001, 2008.

[SGW09] T. Seidel, I. Gasser, and B. Werner. Microscopic car-following models revisited: from road works to fundamental diagrams. *SIAM J. Appl. Dyn. Sys.*, 8 (3):1305–1323, 2009.